HHS Public Access

Author manuscript

Nature. Author manuscript; available in PMC 2013 September 04.

Published in final edited form as:

Nature. 2013 February 28; 494(7438): 484–488. doi:10.1038/nature11889.

Gli activation by aPKC iota/lambda regulates basal cell carcinoma growth

Scott X. Atwood, **Mischa Li**, **Alex Lee**, **Jean Y. Tang**, and **Anthony E. Oro**

Program in Epithelial Biology, Stanford University School of Medicine, Stanford, CA 94305, USA

Abstract

Basal cell carcinoma (BCC) growth requires high levels of Hedgehog (Hh) signaling through the transcription factor Gli[1]. While inhibitors of membrane protein Smoothened (Smo) effectively suppress Hh signaling, early tumor resistance illustrates the need for additional downstream targets for therapy[1–6]. Here we identify atypical Protein Kinase C iota/lambda (aPKC) as a novel Gli regulator. aPKC and its polarity signaling partners[7] colocalize at the centrosome and form a complex with Missing-in-Metastasis (MIM), a scaffolding protein that potentiates Hh signaling[8,9]. Genetic or pharmacological loss of aPKC function blocks Hh signaling and proliferation of BCC cells. aPKC is a Hh target gene that forms a positive feedback loop with Gli and exhibits elevated levels in BCCs. Genome-wide transcriptional profiling shows that aPKC and Smo control the expression of similar genes in tumor cells. aPKC functions downstream of Smo to phosphorylate and activate Gli1, resulting in maximal DNA binding and transcriptional activation. Activated aPKC is upregulated in Smo-inhibitor resistant tumors and targeting aPKC suppresses signaling and growth of resistant BCC cell lines. These results demonstrate aPKC is critical for Hh-dependent processes and implicates aPKC as a new, tumor-selective therapeutic target for the treatment of Smo-inhibitor resistant cancers.

In order to identify new druggable targets in the Hh pathway, we used the scaffold protein MIM, which potentiates Gli-dependent activation downstream of Smo[9], as bait in a biased proteomics screen of factors involved in Hh signaling and ciliogenesis. Two of the hits were polarity proteins not previously linked to the Hh pathway: aPKC, a serine-threonine kinase, and Pard3, a scaffold protein and aPKC substrate (Supplementary Fig. 1a). Reciprocol immunoprecipitation of aPKC and Pard3 pulled down MIM suggesting a specific interaction (Supplementary Fig. 1b). As MIM is a centrosome-associated protein that promotes ciliogenesis[8], we fractionated centrosomes and found aPKC, along with Pard3 and Pard6A, cofractionated and coimmunoprecipitated with MIM in gamma-tubulin positive fractions that mark centrosomes (Fig. 1a; Supplementary Fig. 1c). MIM partially colocalizes with

---

Correspondence and requests for materials should be addressed to A.E.O. (oro@stanford.edu) or S.X.A. (satwood@stanford.edu).

Supplementary Information is linked to the online version of the paper at www.nature.com/nature.

Author Contributions

S.X.A. and A.E.O. designed experiments. S.X.A. performed experiments. M.L. aided in biochemical and knockdown analysis. A.L. and J.Y.T. performed allograft BCC drug treatments. J.Y.T. provided vismodegib-resistant tumor samples. S.X.A. and A.E.O. wrote the manuscript.

aPKC complex members at the basal body in dermal fibroblasts, keratinocytes, and the well-characterized mouse BCC cell line ASZ001[10] (Fig. 1b), where aPKC and MIM interact through coimmunoprecipitation (Fig. 1c). Loss of aPKC or MIM protein suppresses Hh signaling as mRNA levels of Hh target gene *gli1* was reduced and ciliogenesis was inhibited (Fig. 1d,e; Supplementary Fig. 1d,e).

As aPKC kinase activity is necessary for many of its cellular functions[7,11], we used a myristoylated aPKC peptide inhibitor (PSI) to suppress kinase activity[12] (Supplementary Fig. 1f). PSI, but not a myristoylated scrambled peptide, inhibited Hh signaling in BCC cells in a dose-dependent manner similar to the Smo antagonist cyclopamine (Fig. 1f). PSI, a pan PKC inhibitor Go6983, or genetic loss of aPKC expression, also resulted in a dose-dependent inhibition of cell growth in BCC cells, leading to cell death as assayed by the MTT assay (Fig. 1g and Supplementary Fig. 1g,h). PSI inhibited BCC cell growth at a concentration similar to that of cyclopamine, with an IC50 of 5uM. Primary cilia were reduced by 50% in PSI-treated BCC cells (Fig. 1e) indicating aPKC activity is critical to both Hh signaling and ciliogenesis in BCC cells. Interestingly, PSI did not affect proliferation in several non-tumorigenic cells (Supplementary Fig. 1i). PSI specifically inhibited aPKC as loss of aPKC in BCC cells in combination with PSI treatment possesses no additional activity to reduce levels of *gli1* or *apkc* mRNA (Supplementary Fig. 1j).

To address whether aPKC's effect on the Hh pathway is direct, we assayed aPKC function in several nonpolar cell lines (Supplementary Fig. 1k,l; not shown). These cells maintained or increased their primary cilia after aPKC knockdown, however, aPKC removal still blocked Hh activation, reducing target gene induction. We conclude that aPKC's effects on Hh signaling are cilia-independent and required for maximal sustained signaling.

As aPKC is necessary for maximal Hh signaling, we next asked if aPKC is overexpressed in BCCs. Indeed, *apkciota* expression, but not *apkczeta*, is specifically upregulated with *gli1* in BCC cells (Fig. 2a). Similar results are found using freshly isolated human BCCs compared to primary human keratinocytes (Fig. 2b). Immunohistochemical staining of human BCCs and normal skin with antibodies recognizing both total and activated aPKC (P-aPKC) show higher levels in invasive and nodular tumors, with P-aPKC showing greater overexpression (Fig. 2c; 4h). Loss of aPKC removes both aPKC and P-aPKC staining in primary mouse dermal cells, indicating the specificity of the antibody (Supplementary Fig. 2).

As aPKC and Hh signaling are required for BCC cell growth, we next asked whether aPKC is a Hh target gene. Activation of Hh signaling in both polarized and non-polarized primary and immortalized cells using Shh-N ligand induces both *gli1* and *apkciota* transcripts (Fig. 2d). Additionally, when we block Hh signaling by treating BCC cells with cyclopamine, *gli1* and *apkciota* transcripts, but not *apkczeta*, are specifically suppressed (Fig. 2g). Three putative Gli1 binding sites[13] are present in the promoter region within 5 kb of the *apkciota* transcriptional start site in mice (Fig. 2e). Chromatin immunoprecipitation (ChIP) with BCC cells overexpressing Flag:Gli1 enrich in regions containing the three Gli1 binding sites (Fig. 2f) indicating that aPKC is a direct target of Gli1. The first two Gli1 binding sites promote expression of luciferase when expressed in BCC cells suggesting these sites are functional (Supplementary Fig. 3). In addition, expression of *pard6a* (aPKC inhibitor) is reduced

whereas *cdc42* (activator) is overexpressed in primary mouse BCC tumors[14] (Fig. 2h). As aPKC is typically found in an inhibited Pard6A complex, less Par6A would result in excessive free and active aPKC whereas more Cdc42 would activate any existing Pard6A-aPKC complexes. Interestingly, when Hh signaling is inhibited with the Smo antagonist Sant-1, *pard6a* transcript levels are elevated and *cdc42* levels are repressed (Fig. 2i) further supporting the idea that Hh signaling promotes aPKC activation. We conclude that aPKC is part of a Hh-mediated positive feedback loop leading to its overexpression in human and mouse BCCs.

To gain insight into aPKC's mechanism of action, we determined whether aPKC-dependent genes in tumors differed from those regulated by Smo. We treated BCC cells with Sant-1 or PSI and performed 3'-end polyadenylated RNA sequencing. 5700 Sant-1-dependent or 4762 PSI-dependent transcripts changed two-fold or greater when compared to control (Fig. 3a). 4325 transcripts overlapped between the inhibitor-treated data sets ($p<1.0\times10^{-300}$) with most transcripts downregulated in both sets (Fig. 3b). Gene ontology terms associated with commonly changed transcripts include cell cycle regulation, protein transport and localization, and cell division (Fig. 3c). Global transcript expression regardless of fold-change showed a strong positive correlation, with a Pearson correlation of 0.495. Comparision with previously published Hh-dependent data sets from mouse medulloblastomas/granular neural precursors (GNPs) or developing mouse limb bud[15,16] reveals substantial overlap (Supplementary Fig. 4a). 321 of the 1077 Gli1 binding sites found in medulloblastomas/GNPs ($p=1.36\times10^{-11}$) and 41 out of 396 ($p=8.92\times10^{-9}$) Gli3 binding sites identified in the developing limb bud overlap with our commonly changed data set. Representative gene expression profiles among the data sets are displayed in a cluster heat map (Supplementary Fig. 4b). Validation of a subset of transcript expression levels using quantitative RTPCR shows that the relative values from our data set closely mirror actual mRNA levels upon drug treatment (Supplementary Fig. 4c,d). These results indicate that aPKC and Smo regulate a common set of Hh target genes in BCCs.

The striking overlap of transcriptional targets suggested that aPKC might regulate Gli transcription factors. To determine where aPKC acts, we added subthreshold concentrations of cyclopamine or PSI to BCC cells. We found only cyclopamine outcompeted SAG-mediated activation (Supplementary Fig. 5a), indicating aPKC functions downstream of Smo. Moreover, aPKC inhibition modestly increases rather than decreases Gli1 stability (Supplementary Fig. 5b), does not affect Gli2 or Gli3 processing (Supplementary Fig. 5c), and does not alter Gli1 nuclear localization (Fig. 3d; Supplementary Fig. 5d), suggesting that aPKC affects Gli activity. Intriguingly, loss of aPKC in mouse fibroblasts results in a Gli1 band with slightly smaller apparent molecular weight (Supplementary Fig. 5e,f). By contrast, loss of MIM, despite primary cilia defects that prevent significant activation of the Hh pathway[8], have more aPKC protein and a Gli1 band with a slightly larger molecular weight, suggesting aPKC modifies Gli1 posttranslationally.

Consistent with the notion of aPKC-dependent alteration of Gli1 activity, aPKC and Gli1 form a complex as recombinant HIS:aPKC and *in vitro* translated (IVT) human HA:Gli1 or HA:Gli1 zinc finger coimmunoprecipitate (Fig. 3e). Purified aPKC directly phosphorylates Gli1 *in vitro* (Fig. 3f), with the majority of the phosphorylation occurring in the zinc finger

DNA binding region of Gli1. Immunoprecipitation of endogenous Gli1 from BCC cells shows PSI-dependent phosphorylation at serine/threonine residues, further supporting an *in vivo* role for aPKC (Fig. 3g). PSI-treated IVT human Gli1:V5/HIS, where endogenous aPKC is inhibited in the reaction, significantly reduced binding to radiolabeled Gli1 target DNA in an electrophoretic mobility assay (Fig. 3h,i). Addition of recombinant aPKC overcame the effects of PSI to rescue Gli1-dependent DNA binding, whereas heat-inactivated aPKC did not (Supplementary Fig. 5g), indicating Gli1 phosphorylation by aPKC is necessary for maximal DNA binding. The phosphorylation state of Gli1 appears critical as higher concentrations of aPKC leads to paradoxically decreased DNA binding (Supplementary Fig. 5g). We performed a mutagenesis screen of the DNA binding domain to determine the site of aPKC phosphorylation and found that residues S243 and T304 appear to mediate aPKC effects. Phospho-mimetic Gli1 ($Gli1^{S243E,T304E}$) bound to target DNA just as well as wild-type Gli1, whereas phospho-deficient Gli1 ($Gli1^{S243A,T304A}$), which accumulates less aPKC phosphorylation (Supplementary Fig. 5h), has reduced DNA binding ability (Fig. 3h,i). Moreover, $Gli1^{S243E,T304E}$ possesses reduced sensitivity to PSI in BCC cells, suggesting these sites are functional aPKC sites (Fig. 3j). To confirm aPKC regulates Gli binding *in vivo*, we performed ChIP of Flag:Gli1 in BCC cells using Gli target genes[17,18]. On all Gli1 targets assayed, PSI-treated tumor cells left Gli1 nuclear protein levels unchanged but reduced the association with chromatin (Fig. 3d,k). Non-Hh target genes were left unchanged by PSI treatment. We conclude that aPKC regulates Hh signaling by phosphorylating and activating Gli1 to increase its affinity for DNA, illustrating a rare instance where posttranslational modification of a zinc-finger domain promotes DNA binding and transcriptional activity.

To explore whether aPKC inhibitors can be used successfully as a BCC therapeutic, we topically treated allografted BCC tumors[14] with PSI. This tumor model faithfully reflects human BCCs and has previously been used to validate Hh pathway inhibitors now in clinical use[19]. In allografted BCCs, *gli1* mRNA was reduced with increasing concentrations of topical PSI (Fig. 4a). Tumor size was also suppressed with intermediate concentrations of PSI with no apparent acquired resistance (Fig. 4b), comparing favorably with treatment of intermediate concentrations of Smo antagonist itraconazole[19] or Gli2 inhibitor arsenic trioxide[20] (Fig. 4c). Tumors lost their classical palisade patterning upon PSI treatment and apoptosis increased (Supplementary Fig. 6). Cell proliferation was reduced along with Gli1 protein levels. Mice treated with topical or intraperitoneal PSI displayed no apparent adverse effects (Supplementary Fig. 7) except a mild hair cycling phenotype (not shown) suggesting aPKC treatment is tumor-selective.

Because aPKC acts downstream of Smo, we determined whether PSI could inhibit cell growth of Smo-resistant tumors. Following methods to generate resistant lines for other chemotherapeutics like K-ras or B-raf[21], we generated multiple independent BCC cell lines that were resistant to high levels of Sant-1. These Smo-resistant lines displayed increased expression of *apkc* mRNA and protein, with varying levels of *gli1* mRNA (Fig. 4d; Supplementary Fig. 8a). Other Hh target genes displayed differential expression patterns that followed *gli1* or *apkc* mRNA levels, or were generally suppressed (Supplementary Fig. 8b). We verified Smo resistance by treating the cells with high concentrations of structurally

unrelated cyclopamine and found little effect on cell proliferation (Fig. 4e). Treatment of these lines, or Sant-1 sensitive parental lines, with PSI dramatically reduced cell proliferation, suggesting active aPKC plays a role in Smo inhibitor-resistant human tumors. Comparison of Smo inhibitor-sensitive and resistant locally invasive human BCCs, several of which lacked Smo and Sufu mutations as well as Gli1/2 amplification (B. Yauch, personal communication), displayed elevated levels of active aPKC with polyclonal and monoclonal antibodies, corroborating the increase of active aPKC levels as a mode of resistance (Fig. 4f,g; Supplementary Fig. 8c,d). Taken together, these data argue that BCCs become dependent on aPKC to drive Hh activation and tumor growth, and suppression of aPKC activity is sufficient to prevent BCC progression in both Smo sensitive and resistant lines. Our results highlight aPKC inhibition as a viable, tumor-selective alternative to Smo inhibitors to treat Hh-dependent and Smo-resistant cancers.

Full Methods

Tumor immunofluorescence

Human tumors from Smo inhibitor sensitive and resistant patients were obtained from patients enrolled in clinical trials performed by the Stanford group (AEO, JYT), clinical trials NCT00833417 and NCT00957229. Patients were consented under an approved Stanford IRB protocol (#18325). Active and total aPKC levels in human tumor sections were determined by immunofluorescence using rabbit anti-aPKC (1:250; Santa Cruz Biotechnology), rabbit anti-p-aPKC Thr 410 (1:100; Santa Cruz Biotechnology), or mouse anti-p-aPKC Thr 410 (1:100; Santa Cruz Biotechnology). Confocal images were acquired on a Leica SP2 AOBS Laser Scanning Microscope with a HCX PL APO 63× oil immersion objective. Average pixel intensity over five distinct areas per tumor section was determined using ImageJ. Images were arranged with ImageJ, Adobe Photoshop, and Adobe Illustrator.

Cell culture

Primary mouse dermal cells were isolated as previously described[8]. Dermal cells were grown in Amniomax media containing supplement and antibiotics (Invitrogen). ASZ001 cells were grown in 154CF media containing 2% chelated FBS, HKGS supplement, and antibiotics (Invitrogen). Keratinocytes (HPA Culture Collections) were grown in CnT-07 media containing supplement and 0.07mM $CaCl_2$ (CellNTec). Cells were sterum-starved between 24–48 hrs to induce ciliogenesis. MTT cell proliferation assay was performed using manufacturer's protocol from Invitrogen. Cells were transfected with FuGene6 or nucleofected with Amaxa Human Keratinocyte Nucleofector kit using manufacturer's protocol.

Smo resistant cell lines were generated by treating ASZ001 BCC cells with increasingly higher concentrations of Sant-1 every passage for three weeks. Final resistant cell lines were grown in 60uM Sant-1. Cyclopamine was used to inhibit Hh signaling to verify Smo resistance.

Antibodies and immunofluorescence staining

Cells were fixed with either 4% paraformaldehyde or 100% methanol for 10 min. 1% normal horse serum and 0.1% Triton X-100 in PBS was used for blocking. Tissues were fixed with 4% paraformaldehyde and embedded in paraffin. 10um sections were cut and deparaffinized using standard conditions before staining. Tissue sections were blocked using 20% normal horse serum and 0.1% Triton X-100 in PBS. The following antibodies were used: rabbit anti-aPKC (1:500; Santa Cruz Biotechnology), rabbit anti-p-aPKC Thr 410 (1:100; Santa Cruz Biotechnology), mouse anti-p-aPKC Thr 410 (1:100; Santa Cruz Biotechnology), rabbit anti-Pard6a (1:100; Santa Cruz Biotechnology), mouse anti-Pard6a (1:100; Santa Cruz Biotechnology), mouse anti-Pard3 (1:500; Millipore), mouse anti-Cdc42 (1:500; Santa Cruz Biotechnology), rabbit anti-MIM (1:1000)[8], rabbit anti-γ-tubulin (1:500; Sigma), mouse anti-γ-tubulin (1:500; Abcam), mouse anti-acetylated tubulin (1:2000; Sigma), goat anti-Gli2 (1:500; R&D Systems), goat anti-Gli3 (1:250; R&D Systems), rat anti-HA (1:1000, Covance), rabbit anti-KI67 (1:200; Lab Vision), mouse anti-Gli1 (1:1000; Cell Signaling), rabbit anti-phosphoserine/threonine (1:1000; Abcam), mouse anti-actin (1:5000; Sigma), rabbit anti-HSP90 (1:200; Santa Cruz Biotechnology), mouse anti-p63 (1:200; Santa Cruz Biotechnology), and TUNNEL stain (Roche). Secondary antibodies were from Invitrogen. Confocal images were acquired on a Leica SP2 AOBS Laser Scanning Microscope with a HCX PL APO 63× oil immersion objective. Images were arranged with ImageJ, Adobe Photoshop, and Adobe Illustrator.

Protein purification and binding experiments

All proteins were expressed and purified as previously described[22]. *In vitro* translated proteins were produced using manufacturer's protocol in rabbit reticulocyte lysate from Promega. Endogenous proteins were immunoprecipitated by using 5ug rabbit anti-aPKC, chicken anti-MIM, mouse anti-Pard3, rabbit anti-Pard6a, rat anti-HA, mouse anti-Gli1, or mouse anti-Flag (Sigma) with protein A/G-conjugated beads according to the manufacturer's protocol (Santa Cruz Biotechnology). *In vivo* phosphorylated Gli1 detected by immunoprecipitation of Gli1 from BCC cells treated with 10uM MG132 in the presence or absence of 10uM PSI for 6 hrs. Samples were separated by SDS-PAGE and transferred to nitrocellulose, followed by antibody incubations and visualization using chemiluminescent substrate (ThermoScientific).

Centrosomes were purified from mouse C3H 10T1/2 cells as previously described[23]. Supernatant fractions isolated by incubation of mouse BCC cells with lysis buffer (10mM HEPES pH 7.5, 1.5mM $MgCl_2$, 10mM KCl, 0.4% NP-40) for 2 min on ice. Nuclei were spun down and washed twice with lysis buffer before equal volume resuspension in PBS and addition of SDS loading buffer.

Kinase assays

HIS:aPKC (Abcam) was incubated with GST, GST:Gli1, or GST:Gli1 fragments at 30°C for 15 min in kinase reaction buffer (20mM Tris-HCl pH 7.5, 10mM $MgCl_2$, 1mM DTT, 10mM ATP) with 20nM [□-^{32}P]ATP. The reaction was quenched by addition of SDS loading buffer and heated at 95°C for 10 min. The protein was resolved by SDS-PAGE and exposed to a phosphor screen (Molecular Dynamics) and imaged with GE Typhoon 9410.

Luciferase assays

ASZ001 cells were nucleofected (Amaxa) with pGL3-Basic (Promega) containing the following Gli binding sites or mutant sites multimerized (6×) head-to-tail: site 1 (GACCCCCAA); site 1 mutant (GAAACACAG); site 2 (TGCCCCCCA); site 2 mutant (TGAACACCT); site 3 (TACCCCAAA); site 3 mutant (TAAACATAG); glics (GACCACCCA); glics mutant (GATAATCCG). Nucleofected cells were grown to confluency, lysed, and luciferase expression was determined using the Dual-Luciferase Assay System (Promega) and a TD-20/20 Luminometer.

Lentiviral knockdown and drug treatments

Lentiviral pLKO.1 vector containing short hairpin RNAs (Open Biosystems) to prkci (sh3:CCGTTCACCATGAAATGGATA, sh5:CCAGACAGAAAGCAGGTTGTT), or pSicoR-puro vector containing shRNA to MIM[8] were used. Lentivirus containing empty vector pSicoR-puro was used for control knockdowns. Lentiviral infection was performed and cells assayed after three days for prkci shRNA and four days for MIM shRNA. Protein knockdown was confirmed by western blot or qRTPCR.

Drug treatments for cells were performed with myristoylated PSI (myr-SIYRRGARRWRKLY), myristoylated scramble peptide (myr-RGIRYRLRARSWK), Sant-1 (Tocris Bioscience), cyclopamine (Tocris Bioscience), SAG (EMD), Go6983 (Tocris Bioscience), and cyclohexamide (Sigma). Subconfluent ASZ001 cells were serum-starved and inhibitors added for 48 hrs prior to MTT assay (Invitrogen) and 24 hrs prior to visualize cilia and assay Gli target gene induction. Stability assays performed with ASZ001 preincubated with PSI for one hour before 20ug/ml cyclohexamide addition at various time points. Mouse blood parameters were tested by treating mice topically twice daily with DMSO or 0.8mg/kg PSI dissolved in DMSO for 3 days.

Chromatin immunoprecipitation

Protein-DNA complexes were captured by fixing ASZ001 cells expressing Flag:Gli1 and preincubated 24 hrs with inhibitors, fixed for 10 min with 1% formaldehyde, and quenched with 0.125M glycine for 5 min. ChIP was performed using manufacturer's protocol adapted from Upstate. Briefly, cells were lysed for 10 min at 4°C in lysis buffer (50mM Hepes pH7.5, 140mM NaCl, 1mM EDTA, 10% glycerol, 0.1% NP-40, 0.2% Triton-X100, protease inhibitors [Roche]) and nuclei were pelleted and lysed for 10 min at 4°C in nuclei lysis buffer (10mM Tris-HCl pH 8, 100mM NaCl, 1mM EDTA, 0.5mM EGTA, 0.5% N-lauroylsarcosine, protease inhibitors) to obtain DNA. DNA was sheared to a range of 100–600bp in size by sonicating for 25 min. ChIP-grade Flag antibody-conjugated magnetic beads (Sigma) was incubated with nuclei lysate overnight at 4°C. Beads were washed in RIPA buffer and DNA was reverse crosslinked by incubation at 65°C overnight in elution buffer (50mM Tris-HCl pH8, 10mM EDTA, 1% SDS). RNA and protein was digested with RNase A (0.2ug/ml; 37°C for 2 hrs) and proteinase K (0.2ug/ml; 55°C for 2 hrs), respectively, and DNA purified by phenol chloroform extraction using standard protocols. Relative fold enrichment was determined by adding DNA to Brilliant II SYBR Green qPCR Master Mix Kit (Agilent Technologies) containing primers to known Gli target sites listed in

Supplementary Table 1. ChIP with Flag antibody-conjugated magnetic beads in ASZ001 without Flag:Gli1 was used as a negative control.

3’ end RNA sequencing

Library was generated from ASZ001 cells incubated with or without inhibitors for 24 hrs. RNA purified using TRIzol (Invitrogen) and poly A-RNA selected using the micro-poly(A)purist kit (Ambion). Heat-sheared 200ng mRNA for 12 min at 85°C and performed first-strand cDNA synthesis using Superscript III (Invitrogen) for 1 hr at 50°C. Second-strand synthesis was performed using E. coli DNA Ligase (Invitrogen), E. coli DNA Polymerase I (NEB), and E. coli RNAse H (Epicentre) for 2 hr at 16°C. Added T4 DNA Polymerase (NEB) for an additional 15 min before quenching with EDTA. Purified double-stranded cDNA with MinElute Reaction Cleanup Kit (Qiagen). 3’ A-tailed using Klenow Fragment 3’ to 5’ exonuclease (NEB) for 30 min at 37°C. Ligated Illumina linker using T4 DNA Ligase (Enzymatics) overnight at room temperature. Purified 220–300bp bands using 3% NuSieve GTG agarose (Lonza) and MinElute Gel Extraction Kit (Qiagen). Amplified the DNA using Phusion PCR Master Mix (NEB) and 15 cycle PCR program. Purified 220–300bp bands using 3% NuSieve GTG agarose (Lonza) and MinElute Gel Extraction Kit. Sequenced DNA using Illumina Genome Analyzer IIx.

Aligned 36 bp raw reads with Bowtie using the NCBI37/mm9 reference genome. Differential expression analysis was performed on the 3’ exon with the Cufflinks suite using mouse RefSeq gene predictions as a reference transcriptome. Annotated coding transcripts were filtered for significant expression by a RPKM of 25 in at least one sample set. Transcripts that were two-fold or greater changed in drug-treated samples were hierarchically clustered using the Cluster program and visualized in Java Treeview. Transcripts were validated using Brilliant II SYBR Green qRT-PCR Master Mix Kit (Agilent Technologies) with primers listed in Supplementary Table 1. Two-tail p-value between our gene sets and other gene sets calculated using Fisher’s Exact Test.

Supplementary Material

Refer to Web version on PubMed Central for supplementary material.

Acknowledgements

We would like to thank K. Qun for bioinformatics assistance, J. Kim for archival BCC tissue, A.L.S. Chang and S. Aasi for clinical trial operations, K. Chang for technical assistance, and H. Chang and P. Khavari for critical reading of the manuscript. This work was supported by NIH NRSA 1F32CA14208701 (S.X.A.) and NIH grants AR052785 and AR046786 (A.E.O.).

A.E.O. is a clinical investigator for trials funded by Genentech and Novartis.

References

1. Ng JMY, Curran T. The Hedgehog's tale: developing strategies for targeting cancer. Nat Rev Cancer. 2011; 11:493–501. [PubMed: 21614026]
2. Yauch RL, et al. Smoothened mutation confers resistance to a Hedgehog pathway inhibitor in medulloblastoma. Science. 2009; 326:572–574. [PubMed: 19726788]

3. Buonamici S, et al. Interfering with resistance to smoothened antagonists by inhibition of the PI3K pathway in medulloblastoma. Science Translational Medicine. 2010; 2:51ra70.

4. Dijkgraaf GJP, et al. Small molecule inhibition of GDC-0449 refractory smoothened mutants and downstream mechanisms of drug resistance. Cancer Research. 2011; 71:435–444. [PubMed: 21123452]

5. Chang ALS, Oro AE. Initial Assessment of Tumor Regrowth After Vismodegib in Advanced Basal Cell Carcinoma. Arch Dermatol. 2012; 1–2

6. Atwood SX, Chang ALS, Oro AE. Hedgehog pathway inhibition and the race against tumor evolution. The Journal of Cell Biology. 2012

7. St Johnston D, Ahringer J. Cell polarity in eggs and epithelia: parallels and diversity. Cell. 2010; 141:757–774. [PubMed: 20510924]

8. Bershteyn M, Atwood SX, Woo W-M, Li M, Oro AE. MIM and cortactin antagonism regulates ciliogenesis and hedgehog signaling. Dev. Cell. 2010; 19:270–283. [PubMed: 20708589]

9. Callahan CA, et al. MIM/BEG4, a Sonic hedgehog-responsive gene that potentiates Gli-dependent transcription. Genes & Development. 2004; 18:2724–2729. [PubMed: 15545630]

10. Aszterbaum M, et al. Ultraviolet and ionizing radiation enhance the growth of BCCs and trichoblastomas in patched heterozygous knockout mice. Nat Med. 1999; 5:1285–1291. [PubMed: 10545995]

11. Atwood SX, Prehoda KE. aPKC phosphorylates Miranda to polarize fate determinants during neuroblast asymmetric cell division. Curr. Biol. 2009; 19:723–729. [PubMed: 19375318]

12. Standaert ML, et al. Insulin activates protein kinases C-zeta and C-lambda by an autophosphorylation-dependent mechanism and stimulates their translocation to GLUT4 vesicles and other membrane fractions in rat adipocytes. J. Biol. Chem. 1999; 274:25308–25316. [PubMed: 10464256]

13. Winklmayr M, et al. Non-consensus GLI binding sites in Hedgehog target gene regulation. BMC Mol. Biol. 2010; 11:2. [PubMed: 20070907]

14. Wang GY, et al. Establishment of murine basal cell carcinoma allografts: a potential model for preclinical drug testing and for molecular analysis. Journal of Investigative Dermatology. 2011; 131:2298–2305. [PubMed: 21833014]

15. Lee EY, et al. Hedgehog pathway-regulated gene networks in cerebellum development and tumorigenesis. Proceedings of the National Academy of Sciences. 2010; 107:9736–9741.

16. Vokes SA, Ji H, Wong WH, McMahon AP. A genome-scale analysis of the cis-regulatory circuitry underlying sonic hedgehog-mediated patterning of the mammalian limb. Genes & Development. 2008; 22:2651–2663. [PubMed: 18832070]

17. Vokes SA, et al. Genomic characterization of Gli-activator targets in sonic hedgehog-mediated neural patterning. Development. 2007; 134:1977–1989. [PubMed: 17442700]

18. Po A, et al. Hedgehog controls neural stem cells through p53-independent regulation of Nanog. EMBO J. 2010; 29:2646–2658. [PubMed: 20581804]

19. Kim J, et al. Itraconazole, a commonly used antifungal that inhibits Hedgehog pathway activity and cancer growth. Cancer Cell. 2010; 17:388–399. [PubMed: 20385363]

20. Kim J, Lee JJ, Kim J, Gardner D, Beachy PA. Arsenic antagonizes the Hedgehog pathway by preventing ciliary accumulation and reducing stability of the Gli2 transcriptional effector. Proceedings of the National Academy of Sciences. 2010; 107:13432–13437.

21. Little AS, et al. Amplification of the driving oncogene, KRAS or BRAF, underpins acquired resistance to MEK1/2 inhibitors in colorectal cancer cells. Science Signaling. 2011; 4:ra17. [PubMed: 21447798]

22. Atwood SX, Chabu C, Penkert RR, Doe CQ, Prehoda KE. Cdc42 acts downstream of Bazooka to regulate neuroblast polarity through Par-6 aPKC. J. Cell. Sci. 2007; 120:3200–3206. [PubMed: 17726059]

23. Meigs TE, Kaplan DD. Isolation of centrosomes from cultured Mammalian cells. CSH Protoc. 2008; 2008 pdb.prot5039.

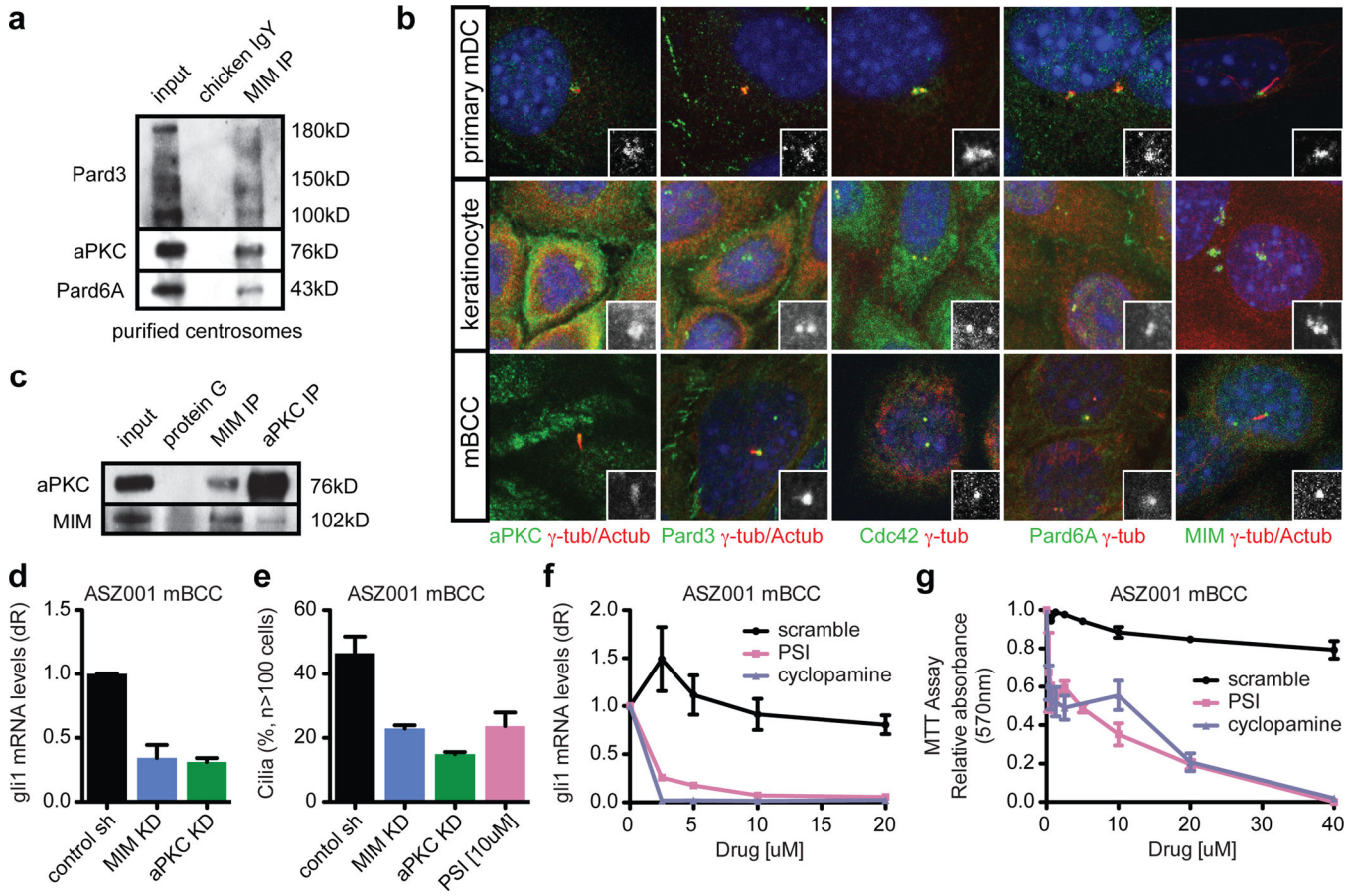

Figure 1. aPKC is a centrosome-associated protein that regulates Hh signaling

a, MIM and aPKC interact in purified centrosomes. **b,** MIM and aPKC complexes localize at the centrosome (γ-tub) versus primary cilia (Actub) of mouse dermal cells (mDC), mouse keratinocytes, and mouse BCC cells. Actub, acetylated tubulin. γ-tub, γ-tubulin. **c,** MIM and aPKC interact in BCC cells. **d–f,** *gli1* mRNA levels (n=3) or cilia percentage (n=3) after MIM or aPKC shRNA, or aPKC or Smo inhibition in BCC cells. sh, short-hairpin. KD, knockdown. **g,** Cell proliferation reduced in BCC cells (n=3) after PSI or cyclopamine treatment, but not myristoylated scrambled peptide. Error bars, s.e.m.

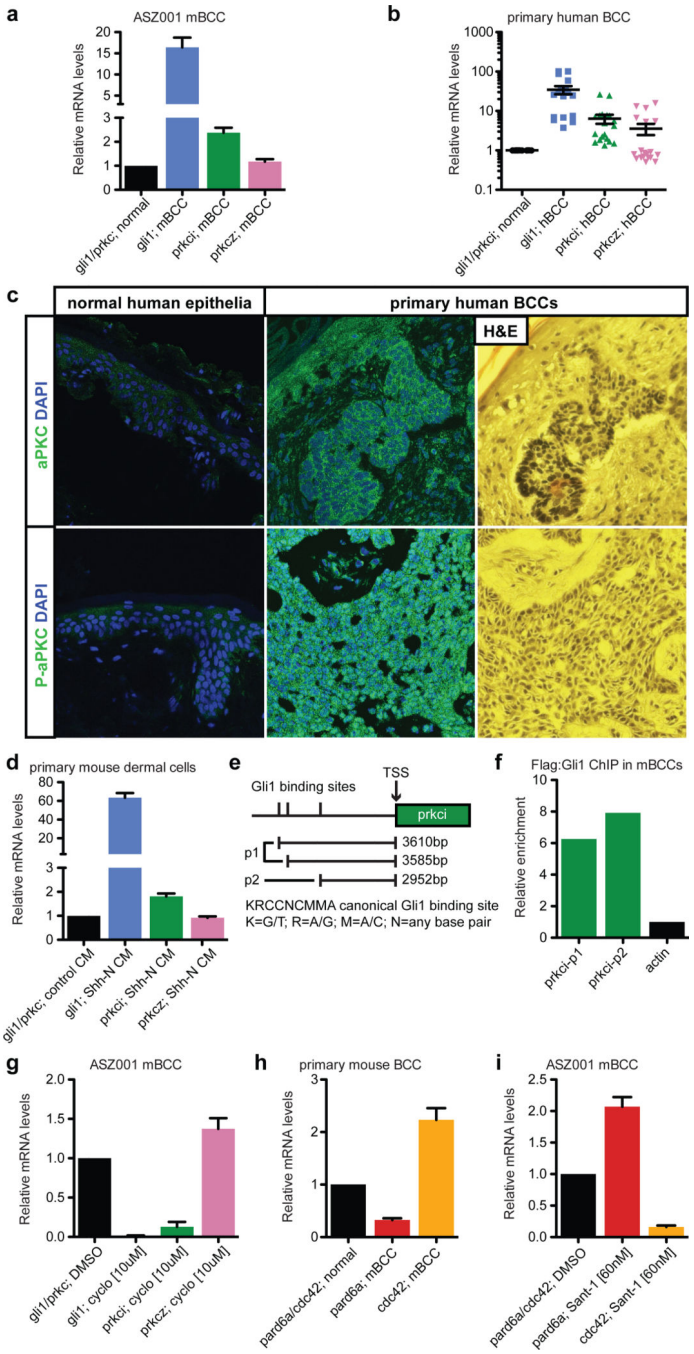

Figure 2. aPKC and Hh form a positive feedback loop in BCCs

a, b, *gli1*, *aokciota*, or *apkczeta* mRNA levels in **(a)** mouse BCC cells (n=3) and **(b)** primary human BCC tumors (n=7). **c,** Total and activated aPKC (P-aPKC) overexpressed in primary human BCC tumors. **d,** *apkciota* is upregulated in Shh-N-treated mouse dermal cells (n=3). CM, conditioned media. **e,** Gli1 binding sites within the promoter region of aPKC. TSS, transcriptional start site. **f,** Flag:Gli1 ChIP of aPKC promoter Gli1 sites. **g,** Cyclopamine suppresses *apkciota* expression in BCC cells (n=3). **h,** *pard6a* expression is reduced and

cdc42 is upregulated in mouse BCC tumors (n=3). **i,** Sant-1-treatment of BCC cells increases *pard6a* and decreases *cdc42* mRNA expression (n=3). Error bars, s.e.m.

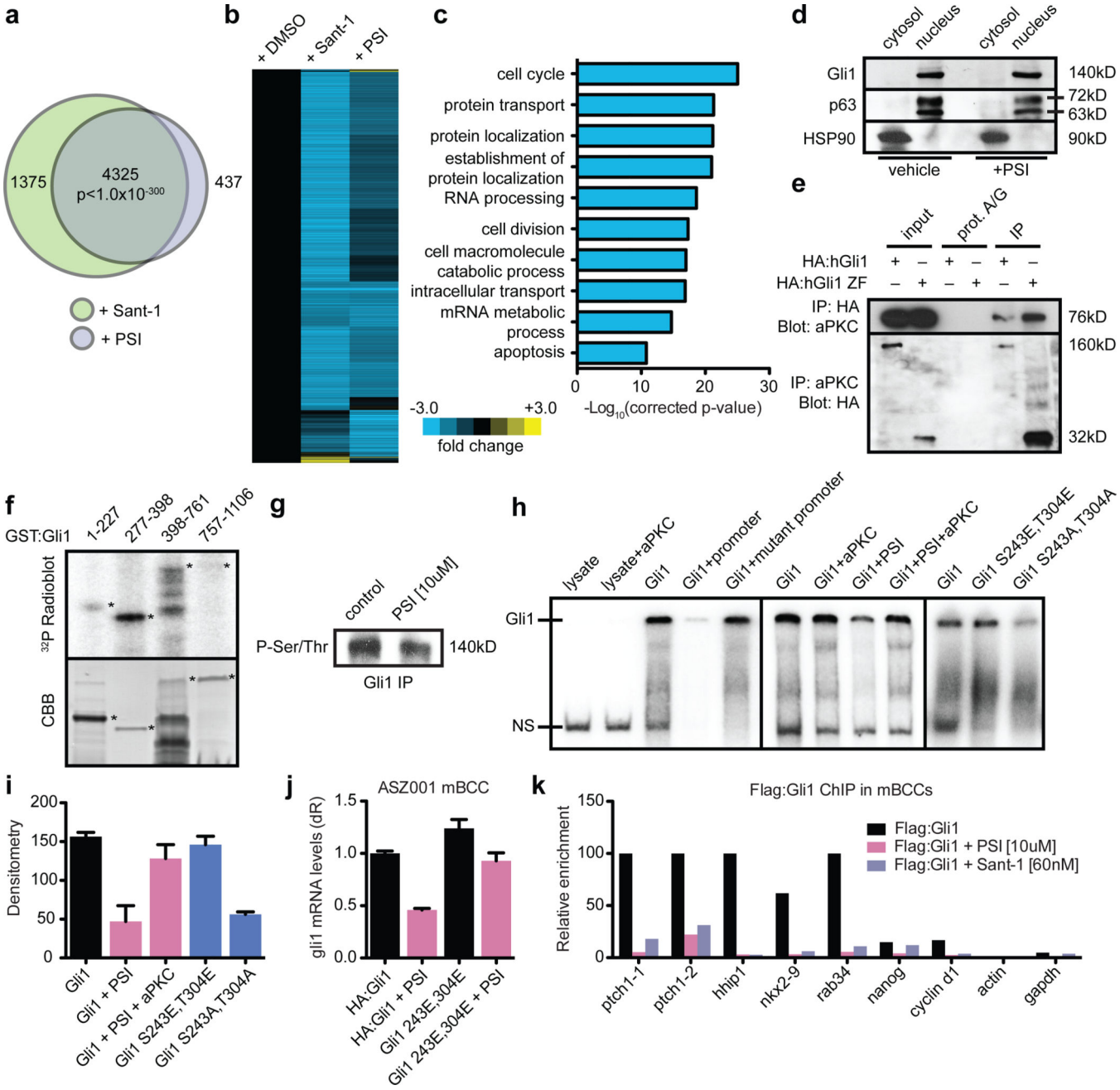

Figure 3. aPKC phosphorylates and activates Gli1

a, Venn diagram and **(b)** heatmap of significantly changed transcripts upon Sant-1 or PSI treatment in BCC cells. **c,** Gene ontology terms of commonly altered transcripts. **d,** PSI does not affect nuclear Gli1 in BCC cells. **e,** aPKC interacts with *in vitro* translated (IVT) human Gli1 or Gli1 DNA-binding domain. **f,** aPKC phosphorylates human Gli1 DNA-binding domain. CBB, coomassie brilliant blue. **g,** PSI reduces phosphorylated serine/threonine levels of immunoprecipitated Gli1 from BCC cells. **h,** aPKC promotes DNA binding of IVT human Gli1 at S243 and T304 in an electrophoretic mobility shift assay (EMSA). NS, non-specific binding. **i,** Densitometry of aPKC rescue, phosphomimetic versus phosphodeficient

Gli1 EMSA (n=3). **j,** BCC cells expressing phosphomimetic Gli1 show reduced PSI sensitivity (n=3). Error bars, s.e.m. **k,** Flag:Gli1 ChIP showing PSI and Sant-1 inhibit Gli1 binding to target chromatin sites in mouse BCC cells.

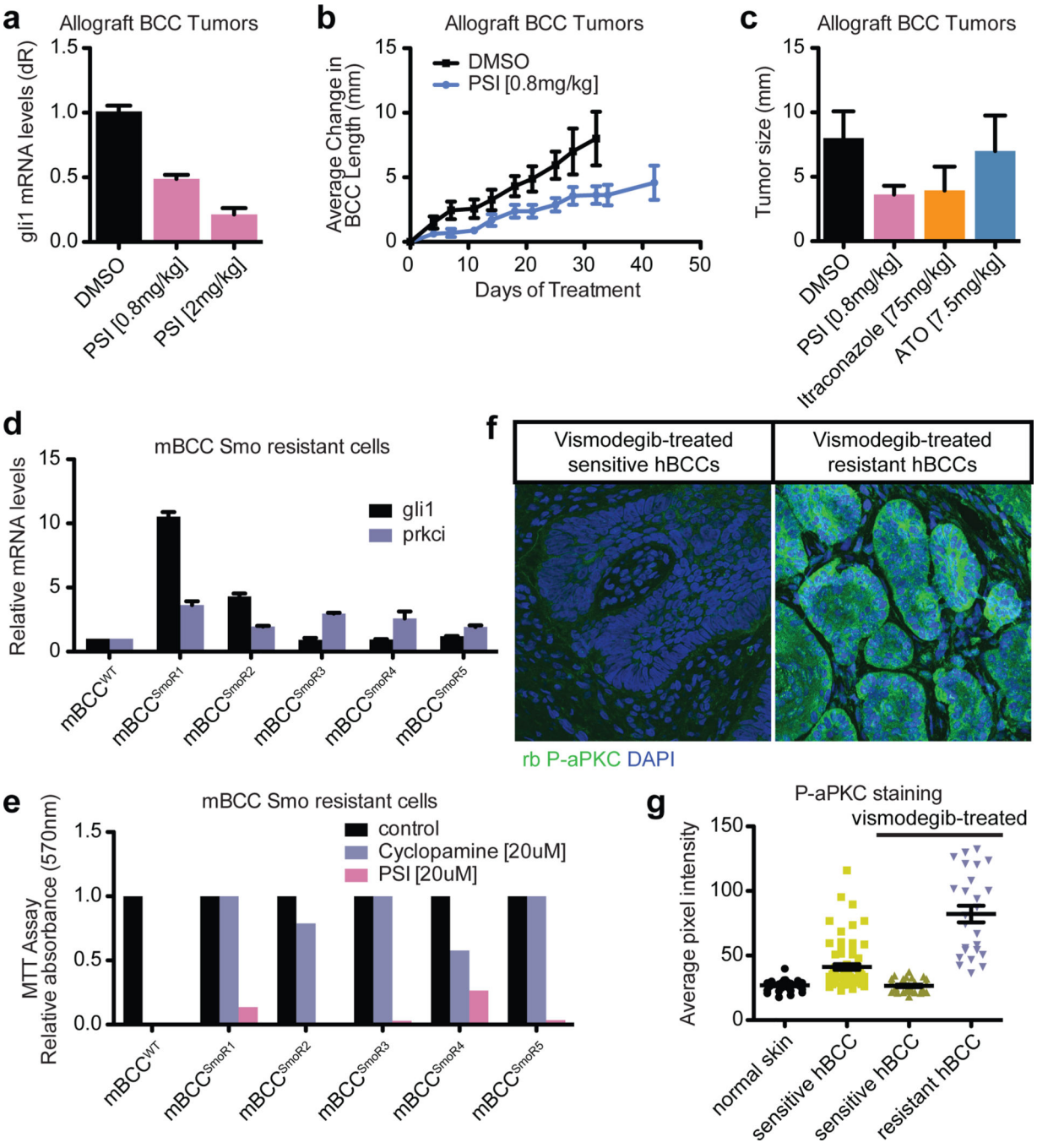

Figure 4. Topical aPKC inhibitor suppresses primary tumor growth

a, PSI inhibits Hh signaling in allografted mouse BCC tumors from Ptch1 +/−, K14CreER2, p53flox/flox mice (n=7). **b,** Topical treatment of allografted BCC tumors slows tumor growth (DMSO n=10, PSI n=9). **c,** Intermediate levels of PSI (n=8) compared to intermediate concentrations of Itraconazole (n=8) and arsenic trioxide (n=5). **d,** Five independently derived Smo-resistant BCC cell lines that amplify *apkc* or *apkc* and *gli1* mRNA levels **(e)** are sensitive to PSI treatment. **f, g,** Vismodegib-treated resistant human BCC tumors (n=6) display elevated levels of active aPKC compared to vismodegib-treated

sensitive tumors (n=8), non-drug treated tumors (n=17), and normal skin (n=7). Error bars, s.e.m.